Journal of Power Sources 248 (2014) 230–238

Contents lists available at ScienceDirect

Journal of Power Sources

journal homepage: www.elsevier.com/locate/jpowsour

Effect of channel materials and trapezoidal corner angles on emerging droplet behavior in Proton Exchange Membrane Fuel Cell gas channels

Preethi Gopalan [a], Satish G. Kandlikar [a,b,*]

[a] Microsystems Engineering, Rochester Institute of Technology, Rochester, NY 14623, USA
[b] Mechanical Engineering, Rochester Institute of Technology, Rochester, NY 14623, USA

HIGHLIGHTS

- Experiments conducted to understand droplet behavior in a trapezoid gas channel.
- At lower air velocities droplet showed corner filling and non-filling behavior.
- At higher air velocities the droplet slid off from the GDL without touching the channel walls.
- Developed model to predict minimum velocity required to remove droplet from channel.
- Model extended to predict ΔP required for corner filling and non-filling cases.

ARTICLE INFO

Article history:
Received 19 August 2013
Received in revised form
13 September 2013
Accepted 16 September 2013
Available online 28 September 2013

Keywords:
Water management
Force balance
Corner filling
Contact angle
Pressure drop
Modeling

ABSTRACT

Ex situ experiments were conducted to study water droplet dynamics in Proton Exchange Membrane Fuel Cell (PEMFC) gas channels with different trapezoid channel open angles and GDL materials under controlled air velocities (0.48–7.23 m s^{-1}). High speed videos revealed that the droplets interacted with the channel walls at lower air velocities (0.48–4 m s^{-1}) and led to channel corner filling depending on the channel open angle. However, at higher air velocities (4.1–7.23 m s^{-1}), the droplets did not contact the channel walls and slid off from the GDL surface. For higher air velocities, a correlation was obtained for the minimum velocity required to remove the droplet from the channel without interacting with the channel walls. For lower air velocities, the minimum pressure drop required for removing the droplet from the gas channel for both corner filling and non-filling scenarios was obtained. The study clearly establishes the important role played by the channel sidewalls and the channel angle on the water droplet transport characteristics.

1. Introduction

Water management in Proton Exchange Membrane Fuel Cells (PEMFCs) has been receiving attention in the automotive sector over the past few years [1–14]. The water removal is particularly challenging at lower gas velocities encountered in the channels during startup and shutdown cycles since the gas velocity is low during these periods. This makes the liquid water removal difficult [1]. Removal of water droplets from the gas channel effectively without lowering the fuel cell efficiency is one of the major issues that needs to be addressed before commercialization of the PEMFCs become a reality in the automotive industry [2].

Over the past few years, a lot of research has been done to address the efficient water removal from the gas channels of the PEMFCs. It has been reported that various factors such as air velocity, channel wall and gas diffusion layer (GDL) material properties, contact angle hysteresis on the GDL and the channel walls, droplet emergence location, and channel cross sectional geometry play important roles in the water removal process [1–23]. It was also revealed that the air flow in the channel exerts pressure force on the droplet which in turn deforms the droplet by changing its contact angle on the channel surface and eventually leads to its removal [9–12].

A droplet or a slug (elongated droplet touching the sidewalls) experiences different forces that act on it and determine its

* Corresponding author. Department of Mechanical Engineering, James E. Gleason Building, Room 09-2001, 76 Lomb Memorial Drive, Rochester, NY 14623-5604, USA. Tel.: +1 585 475 6728.
E-mail addresses: pxg5396@rit.edu (P. Gopalan), sgkeme@rit.edu (S.G. Kandlikar).

0378-7753/$ – see front matter © 2013 Elsevier B.V. All rights reserved.
http://dx.doi.org/10.1016/j.jpowsour.2013.09.070

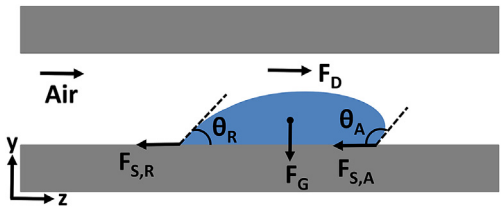

Fig. 1. Different forces acting on the droplet in the PEMFC gas channel.

movement in the gas channel. Fig. 1 shows the different forces acting on a droplet which include gravity (F_g), surface tension ($F\gamma$) and the drag force (F_D) applied due to the gas flow in the channel [24,25]. It is seen that the droplet moves in the gas channel when the gravity and the drag forces overcome the surface tension force holding the droplet in the channel.

The effect of gravity on the droplet (or slug) depends on the size of the droplet. This is generally governed by the Bond number ($B_o = \rho g D^2/\gamma$), which is the ratio of the gravity force to the surface tension force. It is reported that if $B_o \sim 0.1$ or lower, the surface tension forces are dominant in the system and the gravity forces can be neglected [3,26]. Since, the channel size used for gas channels is smaller than about 1 mm, the droplet sizes in the channel are also quite small. Hence, most of the studies in PEMFCs neglect the gravity effect on the droplet. However, it is also seen from a few studies that the gravity does have an effect on the droplet in the PEMFC gas channel [13,22,24,27–29].

Kimball et al. performed a study to understand the effect of gravity on the water movement in the gas channel [24]. They mentioned that the motion of the slug in the gas channel is gravity dependent when the fuel cell is placed vertically. The reactant gas channels are blocked and the current density fluctuates when the slug has to move against the gravity. They also found that the gravity effects were amplified when the large pore for droplet emergence was under the channel region. However, when the large pore was under the land region, the gravity effects diminished [27]. Yi et al. also studied the effect of gravity on the fuel cell performance and concluded that at an optimized gravitational angle for cell orientation, the output power of PEMFC stack can be enhanced greatly [28]. Chen and Wu studied the effect of gravity on water discharge in the PEMFC gas channel [29]. They concluded that the excess water present in the cathode channel is easily removed from the cell when the anode channel orientation is upwards. They also suggested that the placement of anode and cathode is very important for the performance of the PEMFC. Lu et al. studied the effect of orientation of the cell on the water distribution and flow patterns in the gas channels and also found that the vertical orientation of the cell was beneficial for the water flow pattern and the two phase flow in the gas channels as compared to the horizontal cell [22]. Das et al. studied the effect of adhesion force on the liquid water removal from the GDL [13]. They reported that for droplets smaller than 1.5 mm in diameter, the gravity effect can be neglected. However, when the droplet size is above 2 mm or B_o is above 0.14, the gravity has a significant effect on its removal. Therefore, it can be concluded from these studies that the gravity effect in the PEMFC gas channel can be neglected only when the droplet diameter is smaller than 1 mm or B_o less than 0.1, otherwise it needs to be considered in the analysis.

The surface tension forces also play a major role in the droplet removal process. The adhesion force exerted by the surface tension on the droplet is a function of the surface wettability defined by the contact angles (θ) and the contact angle hysteresis ($\Delta\theta$) [30]. Contact angle hysteresis is the difference between the advancing (θ_A) and the receding (θ_R) contact angles. θ_A and θ_R are the maximum and the minimum contact angles respectively that the droplet makes on a surface before it begins to travel on or depart from the surface. When the hysteresis $\Delta\theta$ of a material is high, a larger drag force is required from the air flow in the channel to remove the droplet. When a droplet interface has an angle $\theta < 90°$, it is called a hydrophilic surface and the liquid would spread. An interface having $\theta > 90°$, known as hydrophobic surface, the liquid repels the surface and tries to attain a spherical shape. Droplet removal from a hydrophobic surface is easier as the force required to remove the droplet is less compared to a hydrophilic surface for a given hysteresis. GDL being a hydrophobic surface allows droplet removal relatively easily compared to the hydrophilic channel surface.

Earlier works reported in this area indicate that material properties of the channel sidewall have great influence on the water transport in the gas channel [22,31–34]. It is seen that even though the water moved faster on a hydrophobic surface, having a hydrophobic channel sidewalls is disadvantageous for gas diffusion to the catalyst layer and the fuel cell performance [31]. Quan and Lai performed a numerical simulation to understand water management in the gas channels and found that the hydrophilic channel surface facilitates the transport of reactant gases to the reaction sites by transporting the water along the channel edges [32]. This acts as an effective water management strategy in the gas channels. On the other hand, hydrophilic surface also increases the pressure drop due to liquid water spreading, forming slugs and leading to blockages in the channels. Zhu et al. conducted a numerical study to understand the effect of surface wettability on the droplet removal from the gas channels [33]. They proposed that the hydrophilic channel walls spread water to the channel corners leading to film flow and eventually result in blocking of the gas flow pathways. Similar experimental study was performed by Lu et al. and they found that the hydrophilic channels help in uniform water distribution along the GDL surface [22]. They also stated that hydrophilic gas channel walls help in creating film flow in the channel and therefore reduce the pressure drop in the channel. From all these work it could be seen that both hydrophilic and hydrophobic channels have their merits and demerits.

It was also noted that the channel geometry has an important effect on water management in the PEMFC gas channels. Owejan et al. performed an *in situ* study to understand the effect of gas channel properties on water accumulation in the PEMFCs [15]. They stated that triangular cross-sectional channels retained less amount of water compared to rectangular channels at a given current density. Zhu et al. performed a numerical investigation on six different channel geometries to understand which geometry performs better for a PEMFC gas channel [34]. It was observed that the detachment time, detachment diameter, and removal time of water droplets were found to be lower for triangular and trapezoid channels, and higher for rectangular and upside down trapezoid channels. Similar study was performed by Lu et al., and they reported that sinusoidal and trapezoidal channels produce lower pressure drops in the channel compared to rectangular gas channels [22].

Rath and Kandlikar performed *ex situ* experiments to understand how different angled trapezoid channels affect the droplet dynamics in gas channels from a microscopic perspective [23]. They found that the droplet wicking into the channel corners for a trapezoidal channel depends upon the Concus-Finn condition. According to Concus-Finn condition,

$$2\alpha \leq (\theta_B + \theta_W) - \Pi \quad (1)$$

where θ_B and θ_W is the contact angle for the base and the wall surfaces respectively, and 2α is the channel open angle (angle between the sidewall and GDL) [35–37]. If this equation is satisfied

then the droplet would not wick to the channel corner, whereas when this condition is not satisfied, the droplet would wick to the corner and fill it. Gopalan and Kandlikar extended this work by incorporating air flow in the gas channel [16,18]. They showed that the filling and non-filling behavior of the droplet at the channel corner depends upon the instantaneous dynamic contact angles the droplet makes with the base and the sidewall. They also stated that the pressure drop in the channel for non-filling corners is lower compared to the channels filling the corners. They also investigated the effect of surface properties by experimenting with different channel walls and GDL materials [17,19]. They found that for the commonly employed material pairs used in automotive application, 50° trapezoidal channel acts as the transition angle between filling and non-filling channel corners. Any angle above the transition angle would lead to water wicking to the channel corner and filling it and any angle below the transition angle would lead to no corner filling.

There have been many analytical models proposed in the past to understand the effect of different forces acting on a droplet growing on the base of a microchannel [6–9,38–40]. These models generally employ force balance or torque balance to evaluate the effect of different parameters and membrane properties on droplet formation and its removal. Luca et al. tried to validate these two models with experimental data available in literature and found that the force balance model yields better results when wall shear stress is above 7 Pa and membrane pore diameter is below 1.5 μm [41]. On a similar note, Chen et al. presented a simplified model based on macroscopic force balance and droplet-geometry approximation for predicting the instability in the droplet which leads to its removal from the GDL surface [9]. Zhang et al. performed experimental and analytical studies and developed a correlation for the droplet detachment diameter from the GDL surface in terms of velocity and Reynolds Number (*Re*) [3]. Similarly, Ha et al. also performed experimental study to understand the droplet detachment characteristic from the GDL and complimented it with a simplified model [40]. The model was used as a criterion to estimate the droplet instability and removal tendency in the gas channel.

Hao and Cheng performed numerical simulation using Lattice Boltzman method to understand the influence of gas flow velocity and GDL surface wettability on droplet detachment size and droplet removal time from the gas channel [38,39]. They also developed analytical models based on force balance to predict the droplet detachment size and the shear force required to move the droplet on a hydrophobic wall in terms of dynamic contact angles for a steady velocity profile. Similarly, Cho et al. investigated the dynamics of the liquid water in the PEMFC gas channels through numerical and analytical studies [6,7]. They used CFD simulations to determine the droplet detachment velocity by comparing the wall adhesion and drag forces and proposed an expression relating the Weber number to the Reynolds number. All the above mentioned models are very useful in understanding the droplet behavior in the gas channel, but they all assume that the droplet does not touch the sidewall and do not take into account the channel geometry.

The objective of this work is to study experimentally the droplet dynamics in the PEMFC gas channel with different trapezoidal channel open angle. The experimental study is complimented with analytical models to predict the droplet detachment velocity and the minimum pressure drop required to remove the droplet from the trapezoid gas channels at different air velocities and different open angles. During the experiments, three different types of behavior were observed for the droplet dynamics inside the gas channel. At lower air velocities, the droplet interacted with the channel walls and resulted in channel corner filling or non-filling depending upon the channel open angle [18,19]. At higher air velocities, the droplets were removed from the channel before they touched the channel walls. The model developed encompasses all the different droplet dynamics and is presented in terms of the dynamic contact angles of the channel wall and the base, air velocity, channel open angle, and the droplet emergence or pore location inside the PEMFC gas channel.

2. Experimental study

2.1. Experimental set up

The experimental setup shown in Fig. 2 was developed for an *ex situ* study to understand the effect of air velocity and channel open angle on droplet dynamics in PEMFC gas channels. Since the local water droplet behavior depends only on the local two-phase flow conditions and the channel surface properties, the *ex situ* experiments are expected to provide clear insight on the droplet-wall interactions. The test setup was made up of two plates: (1) the base plate that holds the GDL on the top side and has the water inlet at the bottom as shown in Fig. 2, and (2) the top plate that has the trapezoidal channel of different open angles (45°, 50°, 60°, 90°) etched into it. The top and the bottom plates were made up of polycarbonate material and the length of the gas channel was 100 mm. The hydraulic diameter of the channel was 0.5 mm for all the trapezoidal channels used. The droplet emergence location was 5 mm away from the exit of the channel. A pressure tap was located on the top plate 7 mm away from the exit location of the channel to measure the pressure drop across the droplet. The air flow into the channel was supplied from a Parker Balston HPZA 18000 Zero Air Generator via an air manifold attached to the other end of the channel. The air flow inside the channel was controlled using a rotameter before the air manifold. The experiments were conducted with a Mitsubishi Rayon Corporation GDL (MRC-105 GDL) treated with 6% PTFE and coated with an in-house microporous layer (MPL) at the General Motors facility in Honeoye Falls, NY. The thickness of the GDL was approximately 245 μm. A PTFE gasket of 178 μm thickness was used around the GDL to ensure an appropriate compression.

The test setup was mounted on a vibration isolation table to mitigate any discrepancies due to vibrations. High speed videos at a

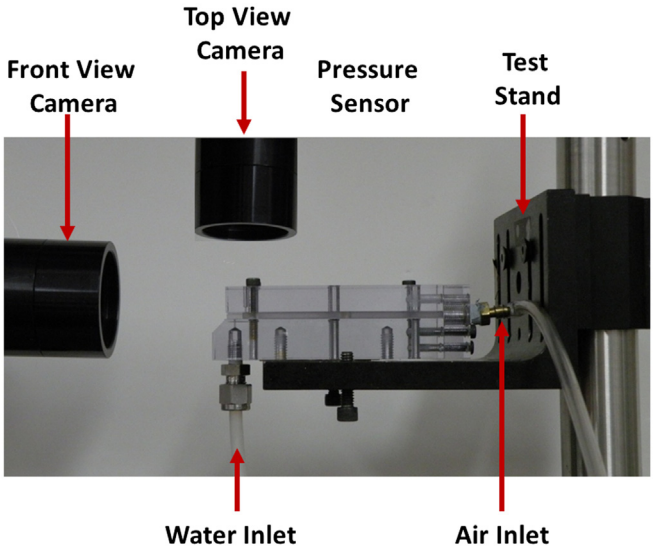

Fig. 2. Experimental set up with high speed camera visualization from both top and front of the channel.

frame rate of 125 fps were recorded to observe the droplet removal pattern from the gas channel using Keyence VW-6000 high speed digital camera. The droplet dynamics in the gas channel were studied previously by the authors for a 3 mm hydraulic diameter channel, which was much larger than the actual fuel cell channel dimensions [18]. Current work was performed to verify those results of channel corner filling behavior and two-phase pressure drop characteristics in a smaller hydraulic diameter channel of 0.5 mm that is representative of actual fuel cell gas channels.

2.2. Experimental details

Experiments were performed with superficial air velocities of 0.48–7.23 m s^{-1}, which correspond to the current densities of 0.1–1.5 A cm^{-2} respectively. These air velocities correspond to an active area of 50 cm^2 in a typical fuel cell for a channel cross section of 0.4 mm × 0.7 mm that meets the Department of Energy specifications [15]. The *Re* for the given air velocities in the channel was within the range of 15–233. Table 1 shows the air velocities corresponding to the current densities and stoich with their respective Re in the gas channel. A Harvard apparatus (Model 11 Plus) syringe pump was used to introduce water on the GDL surface. The water flow rate in the experiments was set at 0.005 ml min^{-1}, which corresponds to a current density of 0.1 A cm^{-2}. The water flow rate does not have any direct bearing on the experiments as the study was focused on the discrete droplet behavior. A preferential pore of 50 μm was made on the GDL such that it was 0.2 mm away from the channel corners for the water to appear at a given location i.e. 5 mm away from the channel exit in the gas channel to facilitate visualization.

The air velocity in the channel was set to the desired value and the water droplet was allowed to grow on the GDL surface until it was removed by the air flow. As the droplet grew in the channel, it interacted with the channel walls differently depending on the channel open angle, contact angles of the water on the GDL and sidewall surfaces, and air velocities introduced in the channel.

The droplet dynamics in the gas channel was captured by the high speed camera from the exit and also from the top of the channel as shown in Fig. 2. The videos were later post-processed using Keyence Motion Analyzer software at 3X magnification. The angles θ, θ_A and θ_R were measured for both the sidewall material and the GDL using a VCA Optima Surface Analysis System before the experiments were performed. Using these values the $\Delta\theta$ values for channel wall and the GDL were calculated. The angles θ, θ_A, θ_R and hysteresis $\Delta\theta$ for the GDL and channel wall material used are given in Table 2.

Concus–Finn condition was used to estimate the transition angle between non-filling and filling conditions of the channel corners for a given material pair. It was found that for MRC-105 GDL and polycarbonate channel wall the transition angle was 50°. The corner filling of the channel is not desirable since the droplet pinned to the channel corners act as viable pinning sites for other successive droplets emerging in the channel. Once the droplets merge with each other, they formed film flow in the channel and eventually lead to slug flow with complete channel blockage. Thus, corner filling is seen undesirable to prevent such degenerative effects.

Table 1
Air velocities corresponding to the current densities and stoic with their respective Re in the gas channel.

Current density (A cm^{-2})	Stoichiometry	Air velocities (m s^{-1})	Reynolds number (*Re*)
0.1	2	0.48	15.53
0.1	3	0.72	23.30
0.2	2	0.96	31.07
0.4	2	1.93	62.13
0.6	2	2.89	93.20
0.8	2	3.85	124.26
1.0	2	4.82	155.33
1.1	2	5.30	170.86
1.3	2	6.26	201.93
1.5	2	7.23	233.00

Table 2
The static, advancing, receding contact angles and hysteresis value for different GDL and channel wall materials used.

Material	Contact angle (θ)	Advancing contact angle (θ_{adv})	Receding contact angle (θ_{rec})	Hysteresis ($\Delta\theta$)
Polycarbonate	80	85	61	24
MRC-105	145	148	138	10
TGP-H-060	142	145	127	18
SGL-25BC	144	148	136	12

3. Results

As stated earlier, the *ex situ* experiments were performed with a 0.4 × 0.7 mm polycarbonate gas channel and MRC-105 GDL under different air velocities (0.48–7.23 m s^{-1}) and trapezoidal channel open angles (45°, 50°, 60°, 90°). Droplet behavior in the gas channel of different open angles was captured from the front view, i.e. from the exit of the channel. For air velocities between 0.48 and 4 m s^{-1}, droplets behaved differently for different open angles. In 90° and 60° channels, it was observed that the droplet filled the channel corners for air velocities below 4 m s^{-1}. Fig. 3 shows the images of corner filling/non-filling behavior observed for different channel open angles at air velocities of 0.72 m s^{-1} and 3.85 m s^{-1}. From the figure it is observed that for 45° channel, the droplet did not fill the channel corners for air velocities below 4 m s^{-1}. However, for 50° channel, different droplet dynamics are observed at different air velocities. For air velocities between 0.48 and 1 m s^{-1}, the droplet led to corner filling behavior, but for air velocities between 1 and 4 m s^{-1}, the droplet showed no corner filling behavior.

Droplet interaction with the sidewall was also visualized from the top of the channel. From this view, the length of the film or the slug flow along the channel cross section was measured. Fig. 4 shows a film and a slug flow pattern in the gas channel from top view for 90° and 50° channels. Using these images, the channel blockage percentages along the channel cross section for 90° and 50° channels were calculated and are shown in Table 3. It is observed from the table that for lower air velocities (0.48–1 m s^{-1}), the droplet completely blocked the channel and formed slug flow. As the air velocity was increased above 1 m s^{-1}, the channel blockage percentage went down and the water flow pattern in the channel transformed into film flow.

A pressure sensor was also connected to the gas channel through a pressure tap placed upstream of the droplet inlet location to measure pressure drop across the droplet. Fig. 5 shows the pressure drop data for different channel open angles as a function of air velocity in the gas channel. It is seen from the figure that the pressure drop increases as the air velocity in the channel increases. Also, it is observed that for a given air velocity, the pressure drop increases with increasing channel open angle. Hence, to predict the pressure drop in a trapezoid channel as a function of air velocity and the channel open angle, a surface plot of the same was developed using Matlab. Figs. 6 and 7 show the pressure drop plots as a function of channel open angles and air velocities for filling and non-filling cases respectively. For both, filling and non-filling cases, similar trends were observed. As the air velocity and the open angle

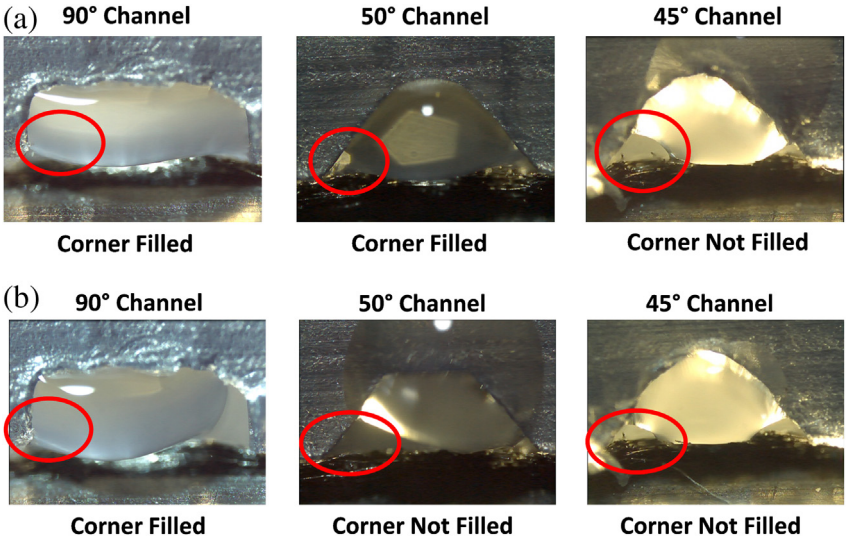

Fig. 3. Images of corner filling/non-filling behavior observed in different channel open angles at air velocity of (a) 0.72 m s^{-1} and (b) 3.85 m s^{-1}.

increases, the pressure drop in the channel goes up. The correlations obtained for pressure drop in terms of air velocity (v) and channel open angle (2α) for channel corner filling and non-filling cases are given by Eqs. (2) and (3) respectively.

$$\Delta P = 46.56\sin 2\alpha + 390.6v^2 - \text{filling} \quad (2)$$

$$\Delta P = 41.33\sin 2\alpha + 261.4v^2 - \text{Non} - \text{filling} \quad (3)$$

These correlations provide the minimum pressure drop required in a trapezoid channel for the droplet to be removed when it interacts with the channel walls at air velocities below 4 m s^{-1}. These correlations for filling and non-filling cases have $R^2 = 0.96$ and 0.95 respectively. These correlations are specific to the channel geometries investigated.

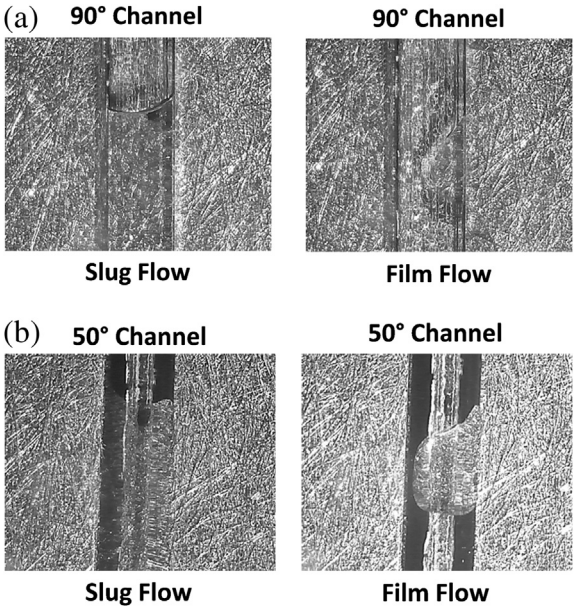

Fig. 4. Image of a film and a slug flow from top view at air velocities of 0.72 m s^{-1} and 3.85 m s^{-1} respectively in a (a) 90° channel and (b) 50° channel.

Droplet dynamics in the gas channel were completely different when the air velocity was increased above 4 m s^{-1}. Fig. 8 shows an image of the droplet removal from a 50° channel at an air velocity of 6.26 m s^{-1}. At very high air velocities (4.1–7.23 m s^{-1}) introduced in the channels with different open angles, it was observed that the droplets slid off from the GDL surface without touching the sidewalls and were removed from the channel. This was mainly because the air velocities were so high that the drag force on the droplet was considerably higher compared to the surface tension force with which the droplet was held on the GDL. To encompass all the forces acting on the droplet at higher air velocities (4.1–7.23 m s^{-1}), a theoretical analysis was performed to determine the minimum droplet detachment velocity required in a microchannel for removing the droplet before it touched the sidewall. The analysis consisted of a force balance on the droplet just before it was moved from the GDL surface. Different forces acting on the droplet in a gas channel are shown in Fig. 9. The gravitational force was neglected in this analysis. As discussed earlier, this assumption is valid for droplets with the Bond number (ratio of gravity to surface

Table 3
Channel blockage percentage for 90° and 50° channels from top view.

Channel open angle	Air velocity (m s^{-1})	Flow pattern	Channel blockage percentage
90	0.48	Slug	100
	0.72	Slug	100
	0.96	Slug	99.75
	1.93	Film	93.33
	2.89	Film	86.67
	3.85	Film	80.67
	4.82	Droplet	72.83
	5.30	Droplet	70.92
	6.26	Droplet	67.66
	7.23	Droplet	64.58
50	0.48	Slug	100
	0.72	Slug	100
	0.96	Slug	99.60
	1.93	Film	86.67
	2.89	Film	80.67
	3.85	Film	78.53
	4.82	Droplet	66.67
	5.30	Droplet	60.40
	6.26	Droplet	55.87
	7.23	Droplet	52.87

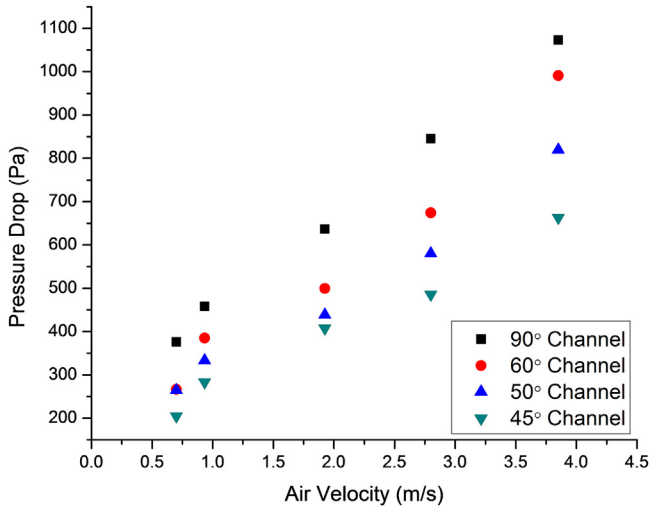

Fig. 5. Pressure drop measured across the droplet in the gas channel for different air velocities.

tension forces) less than 0.1 [13]. For water droplets at standard earth gravity, this result in a limiting droplet radius of 1.5 mm. The droplet sizes in this study were observed to be less than 0.4 mm. It was also observed from Fig. 9 that the drag force acts on the droplet in the direction of air flow whereas the surface tension force which holds the droplet on the GDL acts in the opposite direction. It was also assumed that the drag force, which is the combination of shear force and the pressure force acting on the droplet, was equal and opposite to the net surface tension force at the instance of droplet removal.

$$F_D + F_S = 0 \tag{4}$$

The drag force (F_D) acting on the droplet is given by Eq. (5)

$$F_D = \frac{1}{2} C_D \rho v^2 A \tag{5}$$

where ρ is the density of the fluid applying the force (air), v is the air velocity, A is the area of the droplet on which the drag force is applied and C_D is the drag coefficient on the droplet and it can be estimated using following empirical correlation [3,42].

$$C_D = \frac{24}{Re}\left(1 + 0.1925 Re^{0.63}\right) \tag{6}$$

Eq. (6) is applicable for a spherical droplet. Since the droplet in this case was not completely spherical, this equation cannot be used directly. Also Eq. (6) is applicable for a uniform velocity profile in the channel whereas in this work, the effect of sidewall also needs to be taken into account. Therefore, a rectification factor, K, for the drag coefficient is introduced to account for the effect of the two parameters mentioned earlier.

$$F_D = K \frac{1}{2} C_D \rho v^2 A \tag{7}$$

The area of the droplet on which the drag force is applied was calculated from Fig. 10 using the front view of the droplet. Fig. 10 shows only one of the sidewalls of the gas channel for simplicity. Different parameters shown in Fig. 10 are defined as follows:

θ is the static contact angle of the base wall.
2α is the open angle between the wall and the base.
a is the distance of the droplet emergence location from the channel corner.
β is the inner open angle made by the radius $R_{C1}$with the base of the channel.
b is the vertical distance from the center of the sphere which constitutes the droplet to the base of the channel.
γ is the angle made by the radius $R_{C1}$with the line b passing through the droplet center to the mid- point of the base where the droplet touches.
c is the distance from the center of the droplet to the sidewall such that it makes an angle δ with the radius of the droplet.

The base area of the droplet on the GDL surface was calculated as

$$A = R_{C_1}^2 \left(\theta - \frac{\sin 2\theta}{2}\right) \tag{8}$$

The trapezoid channel open angle is related to the droplet

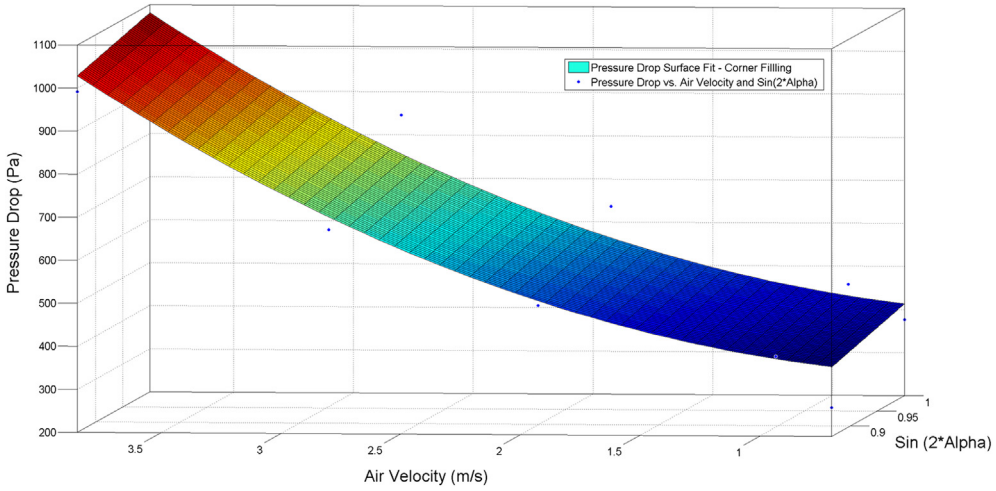

Fig. 6. Pressure drop surface curve in the gas channel as a function of channel open angle and air velocities for filling cases.

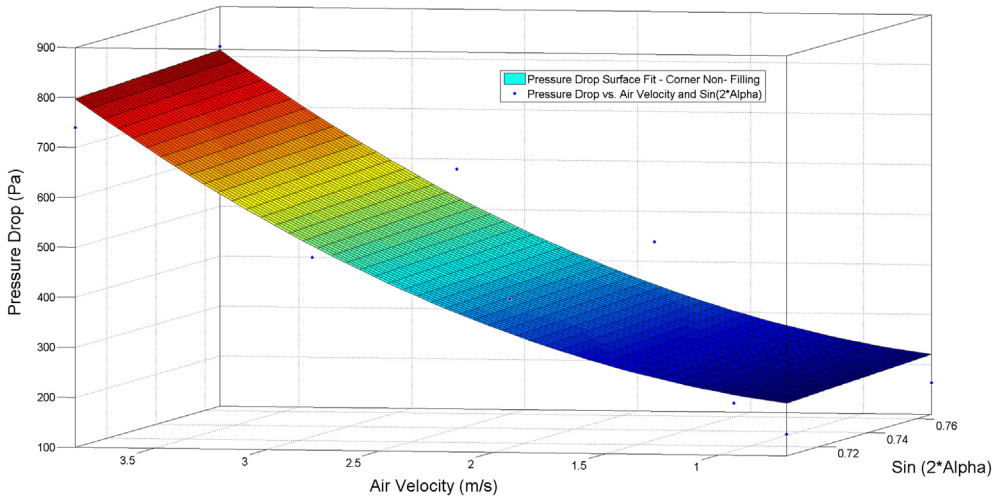

Fig. 7. Pressure drop surface curve in the gas channel as a function of channel open angle and air velocities for non-filling cases.

critical radius (maximum radius of the droplet before it touches the sidewall) as

$$\tan 2\alpha = \frac{R_{C_1}\sin\beta + R_{C_1}\sin\delta}{a - R_{C_1}\cos\delta} \tag{9}$$

From Eq. (9), the maximum radius of the droplet R_{C1} just before it interacts with the sidewall was obtained.

$$R_{C_1} = \frac{a\sin 2\alpha}{1 - (\cos\theta\cos 2\alpha)} \tag{10}$$

Substituting the area of the droplet and R_{C1} in Eq. (7), the drag force applied on the droplet was obtained.

$$F_D = \frac{1}{2} K\, C_D\, \rho\, v^2 \left(\frac{a\sin 2\alpha}{1 - (\cos\theta\cos 2\alpha)}\right)^2 \left(\theta - \frac{\sin 2\theta}{2}\right) \tag{11}$$

Eq. (11) gives the total drag force applied on the droplet by the air flow in a trapezoidal gas channel. To find the K value associated with the droplet dynamics in a trapezoid channel, the drag force is equated to the surface tension force.

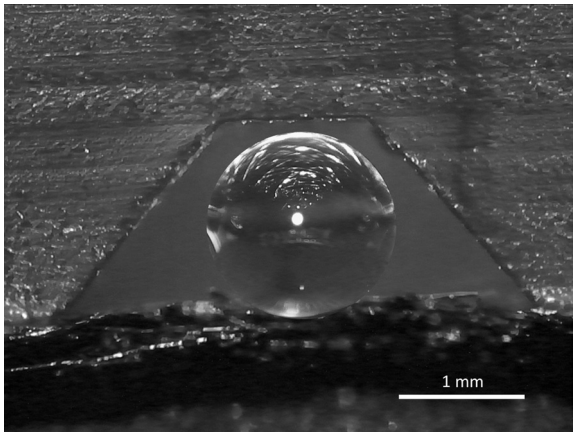

Fig. 8. Image of the droplet removal from a 50° channel without touching the walls of the channel.

The surface tension forces due to advancing ($F_{S,A}$) and receding ($F_{S,R}$) contact angles are given by

$$F_{S,A} = \sigma \cdot 2d \cdot \cos\theta_A \tag{12}$$

$$F_{S,R} = \sigma \cdot 2d \cdot \cos\theta_R \tag{13}$$

where σ is the surface tension coefficient and $2d$ is the width of the contact line (normal to air flow direction) of the droplet on the GDL surface.

The net surface tension force F_S and the width $2d$ are given by

$$F_S = F_{S,A} - F_{S,R} \tag{14}$$

$$F_S = \sigma \cdot 2d \cdot (\cos\theta_A - \cos\theta_R) \tag{15}$$

$$2d = 2R_{C1}\sin\gamma = 2R_{C1}\sin\theta \tag{16}$$

Substituting $2d$ values in Eq. 15

$$F_S = 2\sigma R_{C1}\sin\theta(\cos\theta_A - \cos\theta_R) \tag{17}$$

Substituting R_{C1} value from Eq. (10) in Eq. (17) gives

$$F_S = 2\sigma\left(\frac{a\sin 2\alpha}{1 - (\cos\theta\cos 2\alpha)}\right)\sin\theta(\cos\theta_A - \cos\theta_R) \tag{18}$$

Eq. (18) gives the net surface tension force acting on the droplet holding it on the GDL surface. Combining Eqs. (11) and (18), Eq. (19) is obtained for the minimum velocity required to remove the droplet from the gas channel before it interacts with the channel walls.

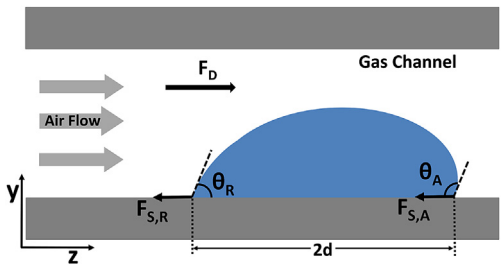

Fig. 9. Image of different forces acting on the droplet in a gas channel.

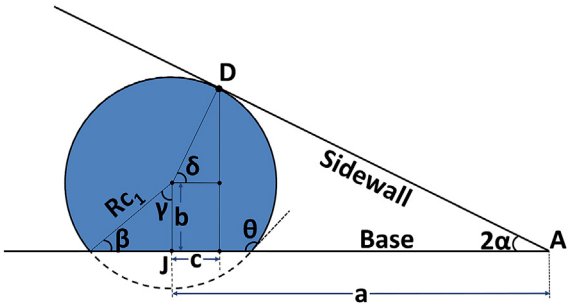

Fig. 10. Area of the droplet on which the drag force is being applied as seen from the front view of the droplet.

$$v = \sqrt{\frac{4\sigma \sin\theta(\cos\theta_A - \cos\theta_R)}{K\, C_D\, \rho\left(\frac{a\sin 2\alpha}{1-(\cos\theta\cos 2\alpha)}\right)\left(\theta - \frac{\sin 2\theta}{2}\right)}} \tag{19}$$

Using the experimental data for the droplet removal from the gas channel, K value was determined for MRC-105 with 5% PTFE. It was seen that the K value varied between 0.7 and 2 for different trapezoid channel open angles and the superficial air velocity in the gas channel.

$$K = (0.65\sin 2\alpha - 0.87)^{*}v + (-6.3\sin 2\alpha + 8.4) - MRC - 105 \tag{20}$$

This K value is also dependent on the GDL material used in the system. Therefore, different GDL materials were also tested in our experiment (TGP-H-060 and SGL-25BC) and their surface wettability properties such as θ, θ_A, θ_R and hysteresis $\Delta\theta$ are given in Table 2. The K values for these GDL materials were also found and are given by Eqs. (21) and (22) respectively. The K values found for different GDL materials based on experimental data and from the theoretical prediction are shown in Fig. 11. It is observed from the figure that the correlation value was within an error of 12% for all the different K values.

$$K = (0.4\sin 2\alpha - 0.66)^{*}v + (-3.88\sin 2\alpha + 6.47) - \mathrm{TGP-H-060} \tag{21}$$

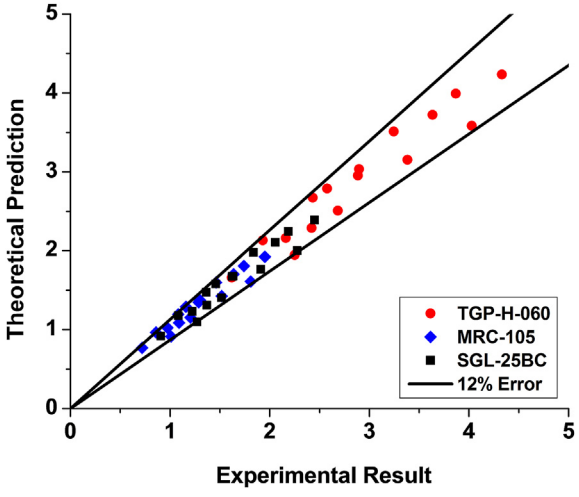

Fig. 11. K values found for different GDL materials based on experimental data and from theoretical prediction.

$$K = (0.88\sin 2\alpha - 1.5)^{*}v + (-8.3\sin 2\alpha + 14.3) - \mathrm{SGL-25BC} \tag{22}$$

This study clearly indicates the important role played by the channel sidewalls and the channel angle on the water transport characteristics. Knowing the previously mentioned parameters for a given system, the minimum velocity required to remove the droplet from the channel before it touches the channel walls can be found using Eq. (19). In addition, if the inlet gas velocity in the channel is known for a given system, the minimum pressure drop required to remove the droplet from the gas channel when the droplet touches the channel walls can be found out using Eqs. (2) and (3).

4. Conclusion

Ex situ experiments were conducted to study the water droplet dynamics in a PEMFC gas channel with different trapezoid channel angles under controlled air velocities of 0.48–7.23 m s^{-1}. High speed videos showing the droplet behavior in the gas channels were obtained and the pressure drop across the droplet was recorded simultaneously. It was revealed through the high-speed videos that the droplet dynamics at the channel corners was significantly influenced by the channel open angles and air velocities. At lower air velocities, droplet led to either channel corner filling or non-filling depending upon the channel open angle. At higher air velocities, the droplets were removed before touching the channel walls. For designing an efficient gas channel design, the minimum pressure drop or minimum velocity of the airflow required in the gas channel for the liquid to be removed efficiently needs to be known. Therefore, a pressure drop correlation was obtained for droplets interacting in a trapezoid channels for both corner filling and non-corner filling scenarios for lower air velocities (0.48–4 m s^{-1}). For higher air velocities, a force balance was performed on the droplet to find the minimum velocity required in a trapezoidal gas channel of different open angles to remove the droplet from the channel before it interacted with the channel walls.

Acknowledgments

This work was conducted in the Thermal Analysis, Microfluidics, and Fuel Cell Laboratory in the Department of Mechanical Engineering at the Rochester Institute of Technology and was supported by the US Department of Energy under contract No. DE-EE0000470. The support from General Motors Electrochemistry Division at Honeoye Falls is gratefully acknowledged.

References

[1] J.T. Gostick, M.W. Fowler, M.A. Ioannidis, M.D. Pritzker, Y.M. Volfkovich, A. Sakars, J. Power Sources 156 (2006) 375–387.
[2] K. Wang, Y.C. Lu, J.H. Xu, G.S. Luo, Langmuir 25 (2009) 2153–2158.
[3] F.Y. Zhang, X.G. Yang, C.Y. Wang, J. Electrochem. Soc. 153 (2006) A225–A232.
[4] C.-Y. Wang, Chem. Rev. 104 (2004) 4727–4766.
[5] J.H. Nam, M. Kaviany, Int. J. Heat Mass Transfer 46 (2003) 4595–4611.
[6] S.C. Cho, Y. Wang, K.S. Chen, J. Power Sources 210 (2012) 191–197.
[7] S.C. Cho, Y. Wang, K.S. Chen, J. Power Sources 206 (2012) 119–128.
[8] A.Z. Weber, J. Newman, Chem. Rev. 104 (2004) 4679–4726.
[9] K.S. Chen, M.A. Hickner, D.R. Noble, Int. J. Energy Res. 29 (2005) 1113–1132.
[10] A. Golpaygan, N. Ashgriz, Int. J. Energy Res. 29 (2005) 1027–1040.
[11] A. Theodorakakos, T. Ous, M. Gavaises, J.M. Nouri, N. Nikolopoulos, H. Yanagihara, J. Colloid Interface Sci. 300 (2006) 673–687.
[12] E.C. Kumbur, K.V. Sharp, M.M. Mench, J. Power Sources 161 (2006) 333–345.
[13] P.K. Das, A. Grippin, A. Kwong, A.Z. Weber, J. Electrochem. Soc. 159 (2012) B489–B496.
[14] J.P. Owejan, J.J. Gagliardo, S.R. Falta, T.A. Trabold, J. Electrochem. Soc. 156 (2009) B1475–B1483.
[15] J.P. Owejan, T.A. Trabold, D.L. Jacobson, M. Arif, S.G. Kandlikar, Int. J. Hydrogen Energy 32 (2007) 4489–4502.
[16] P. Gopalan, S.G. Kandlikar, ECS Trans. 41 (2011) 479–488.

[17] P. Gopalan, S.G. Kandlikar, ECS Trans. 50 (2012) 503–512.
[18] P. Gopalan, S.G. Kandlikar, J. Electrochem. Soc. 159 (2012) F468–F475.
[19] P. Gopalan, S.G. Kandlikar, J. Electrochem. Soc. 160 (2013) F487–F495.
[20] Z. Lu, M.M. Daino, C. Rath, S.G. Kandlikar, Int. J. Hydrogen Energy 35 (2010) 4222–4233.
[21] Z. Lu, S.G. Kandlikar, C. Rath, M. Grimm, W. Domigan, A.D. White, M. Hardbarger, J.P. Owejan, T.A. Trabold, Int. J. Hydrogen Energy 34 (2009) 3445–3456.
[22] Z. Lu, C. Rath, G. Zhang, S.G. Kandlikar, Int. J. Hydrogen Energy 36 (2011) 9864–9875.
[23] C.D. Rath, S.G. Kandlikar, Colloids Surfaces A Physicochem. Eng. Aspects 384 (2011) 653–660.
[24] E. Kimball, T. Whitaker, Y.G. Kevrekidis, J.B. Benziger, AIChE J. 54 (2008) 1313–1332.
[25] J. Lee, J. Hinebaugh, A. Bazylak, Visualizing Liquid Water in PEM Fuel Cells Using X-ray Based Radiography in Through-and In-planes. Meeting Abstracts, MA2013-01, 2013, p. 125.
[26] J.S. Allen, S.Y. Son, S.H. Collicott, Proton exchange membrane fuel cell (PEMFC) flow-field design for improved water management, in: Handbook of Fuel Cells, John Wiley & Sons, Ltd, 2010.
[27] E.E. Kimball, J.B. Benziger, Y.G. Kevrekidis, Fuel Cells 10 (2010) 530–544.
[28] Y. Yi, T. Zheng-kai, Z. Zhi-gang, P. Mu, Int. J. Energy Res. 36 (2012) 845–855.
[29] S. Chen, Y. Wu, Int. J. Hydrogen Energy 35 (2010) 2888–2893.
[30] G. Whyman, E. Bormashenko, T. Stein, Chem. Phys. Lett. 450 (2008) 355–359.
[31] Y.H. Cai, J. Hu, H.P. Ma, B.L. Yi, H.M. Zhang, J. Power Sources 161 (2006) 843–848.
[32] P. Quan, M.-C. Lai, J. Power Sources 164 (2007) 222–237.
[33] X. Zhu, P.C. Sui, N. Djilali, J. Power Sources 181 (2008) 101–115.
[34] X. Zhu, Q. Liao, P.C. Sui, N. Djilali, J. Power Sources 195 (2010) 801–812.
[35] P. Concus, R. Finn, Microgravity Sci. Technol. 7 (1994) 152–155.
[36] P. Concus, R. Finn, SIAM J. Mathematical Analysis 27 (January 1996) 56–69.
[37] P. Concus, R. Finn, Proc. Nat. Acad. Sci. 63 (1969) 292–299.
[38] L. Hao, P. Cheng, J. Power Sources 190 (2009) 435–446.
[39] L. Hao, P. Cheng, Int. J. Heat Mass Transfer 53 (2010) 1243–1246.
[40] T. Ha, B. Kim, H.-S. Kim, K. Min, J. Mech. Sci. Technol. 22 (2008) 1030–1036.
[41] G. De Luca, F.P. Di Maio, A. Di Renzo, E. Drioli, Chem. Eng. Process. Process Intensif. 47 (2008) 1150–1158.
[42] R. Clift, J. Grace, M. Weber, Bubbles, Drops and Particles, Academic, New York, 1978, p. 346.